Silva Rico *et al. Robomech J (2017) 4:8*
DOI 10.1186/s40648-017-0076-4

ROBOMECH Journal

RESEARCH ARTICLE

Open Access

Development of an actuation system based on water jet propulsion for a slim long-reach robot

Jose A. Silva Rico[1*†], Gen Endo[1†], Shigeo Hirose[2†] and Hiroya Yamada[2†]

Abstract

Most of the long-reach inspection devices developed so far have a limitation in the reduction of their diameter when their length is increased. This limitation is due to the technology used to provide the actuation to the system. The use of water-jet as propulsion source is promising to be a solution for this problem. Currently different devices use water-jet as propulsion. However, none of these systems have been designed for small-scale nor have a straightforward control. Therefore, in this paper, we discuss the development of a long-reach water-jet probe aimed to be used in Fukushima Daiichi Nuclear Power Plant. The main elements that define this probe are three high-pressure pumps at the base, three hoses whose water flow is controlled for maneuvering the device, an Inertial Measurement Unit to acquire the attitude of the tip, and a joystick that allows the user the control of the whole device. Moreover, its design allows it to move in different kind of environments and generate three-dimensional motion. Besides the experimentation developed to characterize its behavior, the system was tested in different environments; such as on the ground, in the air and inside the water; showing the best control in aquatic environments.

Keywords: Inspection robot, Long-reach robot, Water-jet propulsion

Background

The incident at the Fukushima Daiichi Nuclear Power Plants (NPPs) has brought different kinds of challenges to the development of robotic devices that are used for decommissioning and cleanup of the installations. Several robots have been used for the decommissioning of reactors in places where accidents have happened, such those employed at Three-Mile Island [1], or for the dismantlement of different facilities around the world due to the end of their lifespan [2, 3], or just for quotidian maintenance labors [4]. All these robots have in common that most of them have been designed to perform certain tasks in environments that are well known or require the preparation of the surroundings to perform their task without problem. Unfortunately, due to the way the accident in Fukushima Daiichi Nuclear Power Plant occurred; earthquake, tsunami, and the hydrogen explosion of the reactor buildings; the infrastructure of the nuclear facility was severely damaged, making it extremely difficult to access critical areas. Ascertaining the exact condition of theses areas has become very complicated. Therefore most of the robots developed up to that moment were not able to be deployed safely inside the facilities.

Debris blocked the access to several areas and many places were flooded due to the tsunami. Various critical locations inside the NPP such as the reactors were inaccessible and their statuses were unknown since many of the measurement instruments were also damaged. This brought severe problems since it was extremely difficult to know the correct way to proceed for the decommissioning and the solution to other important issues, such as stopping the leakage of radioactive material. Before the incident, there were not robots specially designed to deal with this kind of tasks or conditions. For that reason, some of the first robots used to survey the disaster

*Correspondence: silvarico.j.aa@m.titech.ac.jp
†Jose A. Silva Rico, Gen Endo, Shigeo Hirose and Hiroya Yamada contributed equally to this work
[1] Department of Mechanical and Aerospace Engineering, Tokyo Institute of Technology, 2-12-1 Ookayama, Meguro-ku, Tokyo 152-8550, Japan
Full list of author information is available at the end of the article

zone were originally designed to be used on military operations [5]. Although these robots were adapted to be deployed in the disaster area, they faced different difficulties or limitations and the design of more specialized robots became necessary [6].

One of the more alarming situations about the accident was the leakage of radioactive water from the Primary Containment Vessel (PCV). Hence the solution to this problem was a high priority issue in the decommissioning process. The primary challenge with this task is that the accesses to the PCV are limited and not suitable for most of the robotic systems. Furthermore, due to the high level of radiation expected inside of the PCV, the opening of access holes for the insertion of survey systems is not desirable. For that reason, one of the most reasonable access is through the piping system. As is displayed in Fig. 1, a borescope and a thermocouple were inserted through the X-53 penetration pipe in the preliminary investigation at unit 2. After the insertion of the devices to the PVC, they kept hanging next to the wall. Therefore, this investigation only brought data of the conditions of a limited section of the PCV. Figure 2 illustrates the planned route for a more comprehensive inspection of unit 2 with a robotic system. The plan consists in accessing through the X-6 penetration pipe and enter to the pedestal using the Control Rod Drive (CRD) rail. With respect to unit 1, a robot has already been deployed inside the PCV. As is displayed in Fig. 3a, this robot was inserted through the X-100B penetration pipe. After crossing the pipe, the robot along with a monitoring camera were slid hanging inside the PCV until the robot reached the grating. Afterward, the robot conducted an investigation around the grating. All the pipings considered for the investigation consist of straight

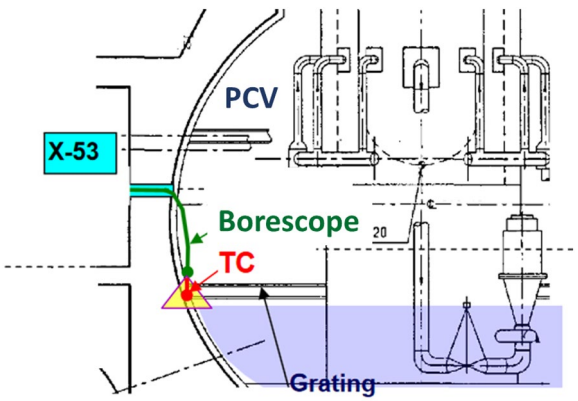

Fig. 1 Access used on preliminary inspection of the Unit 2 PCV. The preliminary inspection inside of PCV was carried out with a borescope (*green*) and a thermocouple (*red*). The access was through a 100 mm inner diameter piping. Adopted from TEPCO [24]

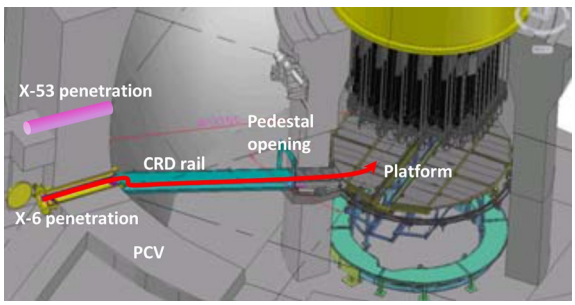

Fig. 2 Different penetration access considered for the investigation in unit 2. The two access route considered are parallel but at different height, since access X-6 may be under the water. Adopted from TEPCO [25]

pipes of about 20 m length and a minimal inner diameter of 100 mm.

The robot deployed in unit 1 is slim enough to access through the piping. It uses crawlers as propulsion elements. Furthermore, as is indicated in Fig. 3b, it is equipped with sensors such as a thermometer, dosimeter, CCD cameras, and laser for measuring distances and is remotely operated by a wired cable. As is shown in Fig. 3c, it is designed to change its form in order to generate better mobility when it reaches the grating. In order to verify the location of fuel debris bellow the grating, it is important the development of a device that can access through the grating whose shortest spacing length is 25 mm [7]. Furthermore, since the current robots are propelled only through crawlers, which require a continuous contact with some surface to properly work, their mobility might be limited in the water contained under the grating. Taking into consideration the condition mentioned before and the limitations of the systems used so far, it is required an inspection system slim and long enough to gain access through the piping and overcome the grating. Moreover, this system must be tough enough to bear radioactivity and aquatic environments, as well as good controllability under water.

Among the different robotic systems available at the moment of the accident, those known as continuum robots seemed to be the best option for this task since these systems are highly adaptable to the surroundings and possess a high length/diameter ratio compare to other systems. Furthermore, in most continuum systems, the heavy actuation elements are placed at their base, enabling the isolation of these components from the harsh conditions of the environment where the inspection is performed and reduction of the weight of the device's inspection segments. In general, these kinds of robots are classified as intrinsic, extrinsic, or hybrid [8]. These classifications are based on the kind of actuation they use. The intrinsic configuration uses fluid in bellows,

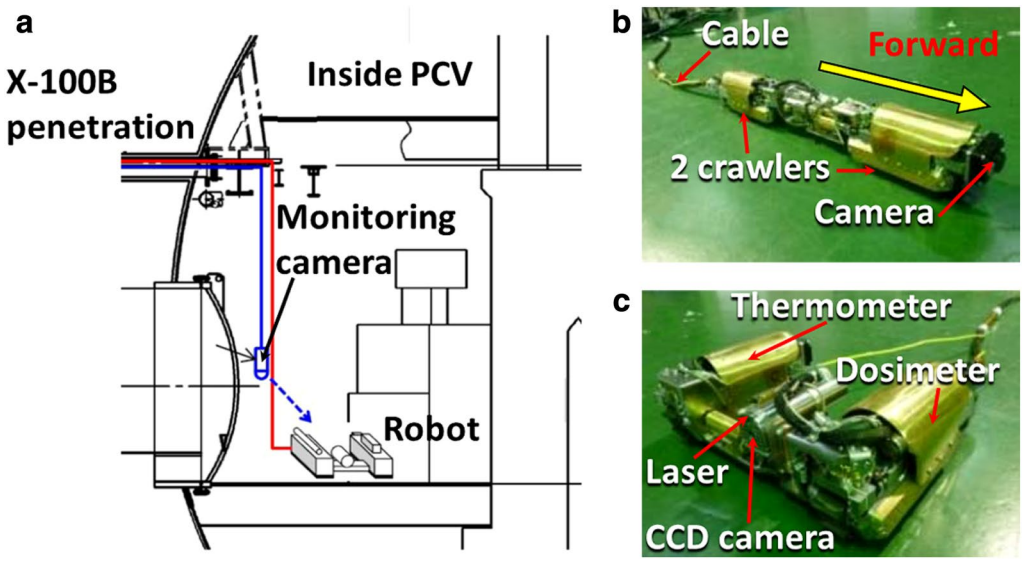

Fig. 3 Access route and system developed inside Unit 1 PCV. **a** Route to access the pedestal in Unit 1 through the penetration pipe of 100 mm inner diameter. **b** Moving through pipe configuration. **c** Moving on granting configuration. Adopted from TEPCO [26]

which allows expansion or contraction by the change of pressure in the fluid. In this manner, the bellow defines the body and actuator element for this system. By the arrangement of at least three bellows in a parallel array, it is possible to generate spatial motion. Additionally, by serially connecting these arrangements, it is possible to build a longer device with more complex locomotion capabilities.

Some examples of this configuration are the systems developed by Festo [9] and the OctArm [10]. On the other hand, the extrinsic configuration is based on bending flexible backbones, such as springs or rods, that are connected at the end of the elements through tendons. These tendons come in triads for every elastic element in order to generate spatial motion. As with the intrinsic systems, several groups of these elements can be connected serially to increase the length and complexity of locomotion. Some examples are the robots developed by OC Robotics [11] and the tendril robot developed by NASA [12]. Finally, the hybrid configuration uses a mix of the systems mentioned before. These combinations could be a concentric/pneumatic, where a flexible backbone is bent through pneumatic actuators instead of tendons; or tendon/pneumatic, where the backbone is based on pneumatic actuators and tendons are used to bend the body [13].

While continuum robots generally have good length/diameter ratios, an increase in the robot's length typically necessitates an increase in the diameter of its proximal part. This is because with every new segment added, more tendons or hoses are required. All these elements have to pass through the body from the base of the system to the segment where are acting. Therefore, the segments nearer to the base tend to be thicker than the rest of the body. This is a disadvantage considering that this task requires a considerably long device that should move inside a 100 mm diameter piping.

OC Robotics has developed a series of snake-arm robots that have been used successfully in NPP to conduct inspection or repair operations [14]. Despite the fact that these robots have high-performance mobility and some of them have diameters smaller than 100 mm, their length is limited to a couple of meters. Another project under development, which also uses wire-rope drive, attempts to increase reach length of the arm. However, the proposed final diameter is not small enough to be deployed through the piping [15]. From the examples mentioned above, the tendril developed by NASA is the only system that keeps a slim constant diameter throughout its length [12]. This is because only a few sections at the distal part are actuated and the rest of the body is passive. This design limits the locomotion of the system and it does not allow controlled propulsion nor locomotion in open areas since the only propulsion force forwards comes from pushing the tendril from its base, where the system is flexible and lacks actuation.

A robotic system that allows the inspection of narrow spaces while keeping a constant diameter all along the device is the active scope camera [16]. This robot has been tested in disaster situations with debris and has shown good performance in adapting to its surroundings. Its propulsion is based on the vibration of its cilia.

However, it requires reasonably good contact with some surface in order to have good propulsion. Taking into account this point, this system would have a limited control or would lose its propulsion due to the lack of contact with surfaces after it exits the access pipe and is inside the water.

Other long-reach systems with a small diameter are those used for the inspection and maintenance of piping networks. The body of these systems is essentially a passive elastic hose, flexible enough to adapt to the continuous change of direction present in pipings, and its propulsion source is located at the tip. This propulsion is based on water-jet which generates enough thrusting force to pull the whole system inside the network. The movement of these devices is limited since their propulsion is only forward; some special passive tools are used to assist in adapting to changing directions [17]. In case the pipe is big enough and path selection is necessary, robotic mechanisms can be employed [18]. Despite the fact that these systems have a fixed diameter along their body and capable of self-propulsion. They lack control for open areas, which is necessary when the system is inside the PCV. There exist other devices that use water-jet as their propulsion source and it is possible to control them in open areas. These devices are developed for amusement activities. Their size is considerably large and their control is completely manual. Furthermore, the user requires highly trained skills, as well as ride the device to control it through his/her body movements [19, 20].

Taking into account all the elements mentioned before, we propose a new robotic system that uses water-jet as a propulsion source. The flow of water-jet is automatically controlled based on the operator's commands and data from a posture sensor, achieving ease maneuvering. The overview of the system is illustrated in Fig. 4. This system is composed of the following items.

1. High-pressure pump. This element is necessary to generate flow through a long and thin hose. By the regulation of the speed of the pump, the flow is regulated, consequently the thrust force as well.
2. Flexible hose. This element allows the transportation of water from the base to the tip of the system. It should be strong enough to bear the pressure required to transport the liquid, as well as flexible enough to allow adaptation to the surroundings. Furthermore, it should be long enough to move through the 20 m length pipe and conduct the inspection inside the PCV.
3. Nozzle. This element is used for the redirection of the flow, as well as to increase the speed of the fluid in order to augment the thrust force of the water-jet.

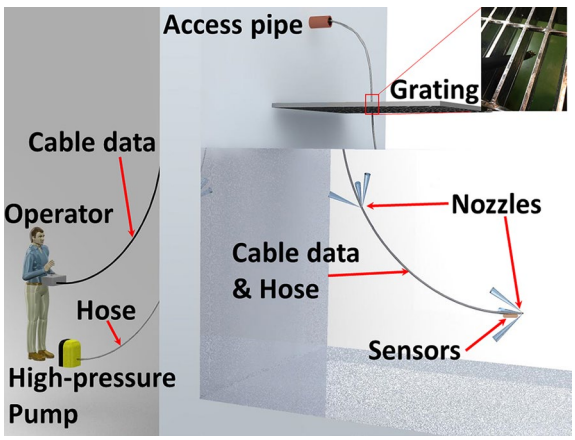

Fig. 4 Concept of the proposed device. The concept establishes an inspection system slender enough to move through the piping and pass the grating inside the PVC and move inside the water. The propulsion of the device is located at the tip of the system and is based on the water-jet propulsion. However, we also consider the implementation of intermediate water-jets to improve the motion

4. Posture sensor. This sensor is to acquire the variations on the attitude at the tip of the device. Data obtained from this sensor is used to adjust the flow of water in order to correct any variation that modifies the operator's commands. Moreover, we consider the addition of more nozzles along the body. These will assist the movement of the system, in case an inspection in a more complex piping is planned. Other sensors such as camera, dosimeter, temperature sensor, and so on, should be mounted at the tip of the probe in order to have a useful inspection system.

The novelty of the concept proposed is that with the combination of inertial sensing and water-jet propulsion, it is possible developing systems highly adaptable to the surroundings, and with a larger length/diameter ratio. As well as the reduction in the number of actuators and an easy control that might not require previous training since inertial sensing helps to solve different issues present in a purely manual control.

In this paper, we center our attention on the study of the feasibility of the water-jet as a propulsion for a slim, long-length inspection system and the analysis of a device potentially capable of fulfilling the requirements of size and mobility necessary for the inspection task inside the PCV. In this first stage of the study, we focused on the propulsion and control at the tip of the device. First, we outline different possible configurations of devices that allow us to verify our proposal and then the theoretical background is formulated. Next, we analyze the results of basic experiments performed in order to understand

the relationship between the different variables and how they affect the propulsive performance of the system. Afterward, considering the results of the characterization of the variables, a first prototype is suggested and the details of its mechanical, electronic and control design are explained. Finally, a discussion and analysis of experiments carried out in order to verify the mobility of the prototype in different environments is presented.

Design concept

We consider the water-jet as a good option to be implemented as propulsion source for a probe since a water-jet can be generated via the transfer of water through a long hose with constant and relatively small diameter from a water source to an output nozzle. Additionally, such a water-jet generates a thrust force that can be controlled by the regulation of the flow rate. Taking into account that this system requires control in open areas, three different configurations are suggested. The first one is a configuration similar to the tendril from NASA with the difference that only one actuated section is required at the tip; in this way, it is possible to position the tip in the desired place in the three-dimensional space. The water-jet is directed partially backwards to the longitudinal axis of the hose, in the same way as in the piping inspection devices, and via the regulation of the flow rate, the magnitude of the thrust force can be controlled. The second option is by regulating the water-jet through servo-valves. Similar to continuum robots, at least three actuation elements are necessary to control the motion in three-dimensional space. Thus, it requires independent control of each water-jet. This necessitates at least three servo valves which should be placed at the tip of the probe in order to regulate the opening of the orifices of each water-jet, thereby controlling the flow rate and thrust force. However, the need of servo valves at the tip will increase the diameter of the device and the complexity of the manufacture. Finally, the last proposal is a device with no mobile element at the tip. Instead, it has three nozzles in circular arrangement directed partially backward. Each water-jet is generated independently, which means that each nozzle has its own feeding hose and independent pump. By regulating the speed of each pump, the flow and thrust force are controlled. Because the last option is the easiest to implement, we chose the three hose configuration to test the concept. A more detailed study of the generation of water-jet thrust force is presented next.

Water-jet thrust

The water-jet thrust has been used in different robotic systems such as unmanned surface vehicles [21], underwater robots [22, 23] and so on. However, these systems require immersion in or direct contact with water because they take the water for their propulsion directly from the environment. It is therefore difficult to reduce their size because their pumps are contained in the main body. Nevertheless, the loss of energy due to the transportation of the water from the input to the output is reduced since these two elements are relatively near to each other. In order to understand how the water-jet propulsion is developed, an idealized nozzle displayed in Fig. 5 is considered. In this diagram, the water enters through the inlet, whose transversal area is A_i, with a velocity v_i and goes out through the outlet, that has a transversal area A_o, with a velocity v_o. Because water is used as the fluid of propulsion and this is considered as an incompressible element, a special case of the continuity equation, where the mass flow rate ($\dot{m}$) is constant, is used in order to describe the relation of the velocities at different points.

$$\dot{m} = \rho v_{\mathrm{i}} A_{\mathrm{i}} = \rho v_{\mathrm{o}} A_{\mathrm{o}} \tag{1}$$

where ρ represents the density of the water.

With Eq. 1, it is possible to deduce that the velocity of the water increases at the output by reducing the diameter of the output. In an ideal case, where the input and output are aligned or in parallel axes, the incremental of the rate of change of the momentum is equal to the thrust generated. Thus, the faster the water flows at the output, the larger the thrust force becomes. However, due to the change of direction of the fluid, more elements need to be considered as is shown in Fig. 6. In this figure, the element of study, the nozzle, is delimited inside a control surface. In this control surface P_i and P_o represent the pressure of the water inside the nozzle and the atmospheric pressure at the output of the nozzle respectively while v_i and v_o are the velocities of the water crossing the control surface at the inlet and outlet respectively. Finally, $\mathbf{F}_T$ is the force necessary to keep the system still and represents the force that cancels the thrust force generated by the effects of the inner pressure and the rate of change of the momentum of the water. The precise direction where $\mathbf{F}_T$ is directed is unknown, however, we consider that most of the thrust force is generated by the water-jet,

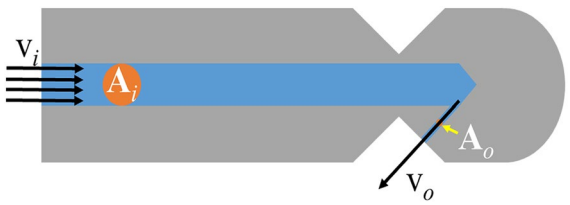

Fig. 5 Flow of water inside the nozzle. V_i and V_o represents the flow of the water and its direction at the input and output respectively. The *oranges circles* A_i and A_o represent the transversal area of the input and output respectively

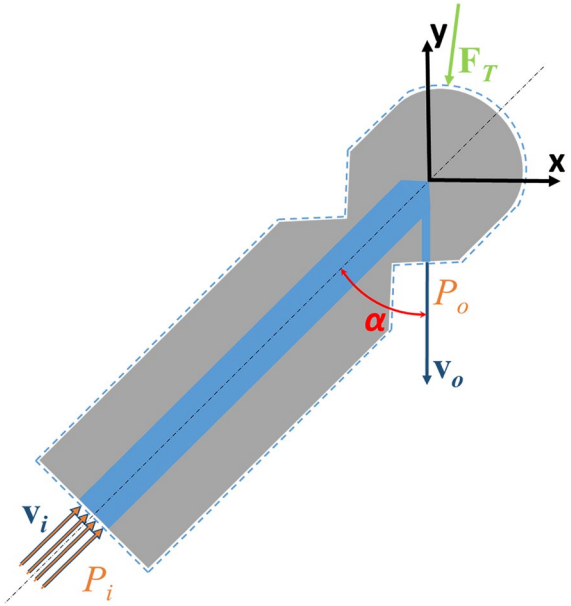

Fig. 6 Description of the variables considerer for the analysis. The elements that generate the thrust force F_T are the pressures P_i, P_o and the flow of water at the inlet and outlet whose velocities are v_i and v_o respectively

therefore, for our analysis the outlet is aligned with the y-axis in order to focus on this direction. For this analysis the momentum equation for inertial control volume for steady fluid is used.

$$\sum \mathbf{F}_s = \int_{CS} \mathbf{v}\rho\mathbf{v} \cdot d\mathbf{A} \tag{2}$$

where $\mathbf{F}_s$ represents the surface forces applied on the control surface. In our case, these forces are $\mathbf{F}_T$ and the forces generated by the pressures P_i and P_o (although P_o can be ignored if gauge pressure values are used). $\mathbf{v}$ is the velocity of the fluid when it crosses the control surface and, finally, $\mathbf{A}$ is the transversal area where the fluid crosses. Developing Eq. 2 with the elements of our system in the y-axis and solving for F_{T_y} we obtain

$$F_{T_y} = {v_i}^2 \rho A_i \cos\alpha + {v_o}^2 \rho A_o + f(P_i) \tag{3}$$

Keeping the system motionless, the right side of Eq. 3 contains the variables that generate propulsive forces that are canceled by $\mathbf{F}_T$ in the y-axis. These variables are: the flows of water at the inlet and outlet, represented respectively by the first and second addend, and the inner pressure of the hose, represented by the last addend of the equation. Taking into account the proposal of the probe done, it is important to consider that these variables are generated at the base of the system and the values considered for the propulsion force are those measured at the nozzle. As mention before, since water is an incompressible fluid, the flow rate remains constant throughout the device, while the pressure of the water decreases from the pump to the nozzle.

Pressure loss

The loss of pressure in the piping is due to the friction of the fluid against itself and its surroundings. Therefore, the loss increases in the direction of the flow and it is directly related to the square of the speed of the fluid inside the pipe. In the case of straight pipes, the pressure loss can be calculated with the Darcy equation, Eq. 4, where ΔP is the pressure loss, ρ the density of the fluid, L the length of the pipe, D the inner diameter of the pipe, v the average velocity of the flow and finally f is a friction factor that is obtained experimentally. The probability of using this expression for our system is unlikely due to the flexibility of the hoses and the conditions of the task. Therefore, a modification of this last expression is done as shown in Eq. 5. This new equation allows the calculation of the pressure loss in valves, fittings, reductions, bends, and so on. The term K, which is known as the resistance coefficient, is calculated through experimentation. Even though the coefficients of many different elements have already been calculated, due to the characteristics of the proposed system, it was necessary to conduct experiments to determine the value of the coefficients.

$$\Delta P = \rho f \frac{L}{D} \frac{v^2}{2} \tag{4}$$

$$= \rho K \frac{v^2}{2} \tag{5}$$

Water-jet experiments

The understanding of the thrust force generated at the tip of the system is crucial because this force is used for the forward propulsion as well as the control of the motion in the space. In our proposal, we suggest the use of three identical water-jet positioned in a circular arrangement. Since they are identical, the experimentation of only one is enough to understand the behavior and with the superposition of the results, it is possible to predict the behavior of the three water-jet together.

Test apparatus

In order to measure the variables involved in the system, such as pressure, mass flow rate, and thrust force, the test apparatus shown in Fig. 7 was built. With this test apparatus, we pursue the reproduction of the main features of the nozzle displayed in Fig. 6. However, this design of the test device considers exchangeable output nozzles and the measurement of the pressure at the inlet of the nozzle as well as at the output of the pump.

It is therefore possible to quantify the pressure drop in the hose. The angle α that describes the direction of the output with respect to the input has a fixed value of 45°. Different diameters of the nozzle are considered for the experiments, ranging from 0.2 to 0.8 mm with an interval of 0.1 mm. The direction of the output of the nozzle is aligned to a shaft that is connected to a force gauge (Shimpo FGP-5) in order to measure the thrust force. From the flow source to the nozzle, a high-pressure hose is used. This hose is comprised of an inner polyester tube that is covered with stainless steel braid. The diameter of the inner tube is 4.5 mm while the external diameter of the stainless cover is 7 mm and the total length of the hose is 5 m. The minimal bending radius recommended for the hose is approximately 25 mm and it can support pressures up to 15 MPa. The water flow is generated by a pump used in a domestic purposes water-jet washing machine (IRIS OHYAMA FBN-401). The specifications of this system are shown in Table 1. Internally, this washing machine uses an axial piston pump of three pistons to propel the water and an electric universal motor which drives the pump. Since the universal motors can operate on AC or DC power, we decided to use DC power to regulate the speed of the motor and consequently, the flow of water varying of the voltage supplied to the motor.

Table 1 Specification of water-jet washing machine

Characteristic	Value
Power supply	AC 100V 50/60 Hz
Regular discharge pressure	Approximately 6.0 MPa
Regular discharge water	Approximately 270 l/h
Power consumption	1000 W
Body weight	Approximately 4 kg

The measurement of the pressure at the two ends of the hose is done via the VESV/VESI series VALCOM pressure transmitters. Meanwhile, the mass flow rate is calculated indirectly through the measurement of the of the mass of the water that is expelled from the outlet and

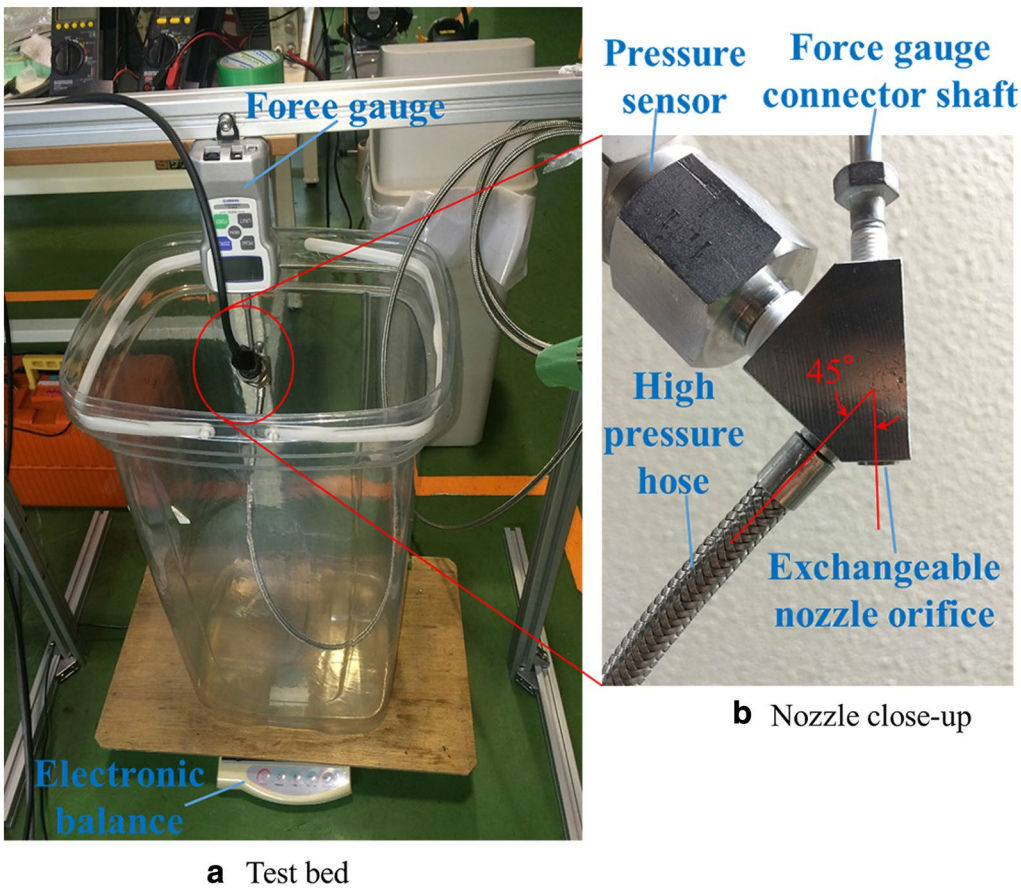

Fig. 7 Experimental test bed. **a** General view of all the elements that define the test bed. **b** Detailed view of the nozzle and the elements attached to it

collected inside a container. The mass of this container is measured with a AJ series Vibra balance.

Mass flow rate measurement

As mentioned before, an electronic balance is used to measure the mass of the container. This balance is configured to acquire the mass every 0.1 s for a period of 6 s. The mass flow is acquired by means of the gradient calculated from the data acquired. The mass flow rate is measured at different input voltages, from 10 to 60 V at an interval of 5 V. The measurement initializes from 10 V because this is the minimal voltage necessary to start the motion of the pump. The experimentation was conducted with all the diameters of nozzle. Figure 8 shows the results of the experiments as well as their trend lines. The relationship between the voltage supplied to the pump and the mass flow can be described through square functions. However, after a certain point, the flow rate becomes constant, even though the voltage continues increasing. This happens when the maximum pressure that the pump is able to generate is reached. The chart also visually indicates that there is a linear tendency in the point where the constant flow starts, which is related to the output diameter of the nozzle. It is important to mention that the flow is reduced with the reduction of the diameter of the orifice. Furthermore, the smaller the diameter of the nozzle, the faster we reached the maximum pressure and with lower voltage.

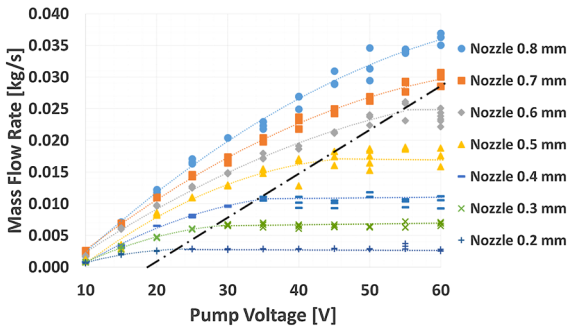

Fig. 8 Description of the mass flow rate generated with different diameters of the outlet at different voltages supplied to the pump. The flow rate mass displayed at the left side of the *dashed line* has quadratic behavior and keeps a constant value at the right side

Pressure measurement

The pressure drop of the water varies depending on the state of the hose. Consequently, the pressure drop in the hose does not have a steady value. Since it is not feasible to obtain a unique friction factor for the hose, we aim to calculate the highest possible value. In order to calculate this value, most of the hose was gathered in a coil of approximately 0.15 m of diameter. We consider that this condition generates one of the highest friction factors that the system could present due to the continuous changes of direction of the flow of water. These changes generate secondary flows along the hose and these augment the friction. The only moment this condition is presented is when the device is collected before being deployed. During the deployment, it is unlikely that this situation happen. Therefore, it is unlikely to generate larger pressure drop values than those calculated on this condition.

During the experimentation, the maximum pressure reached was around 8 MPa, which is larger than the maximum pressure specified by the maker. However, it was possible to reach this value without activating the security pressure switch installed in the pump. Therefore, we presume that the reason for the pressure did not increasing further is due to the mechanical strength limitation of the pump. The behavior of the pressure can be visualized in Fig. 9. The incremental rate of the pressure increases as the diameter of the output get smaller. Furthermore, it is observed that the relationship between the pressure and the voltage can be described by a quartic function before the pressure reaches its maximum value. However, this performance could vary depending on the pump. For that reason, the pressure was evaluated with respect to another variable that is independent of the pump, in this case, the mass flow rate. The behavior of the pressure with respect to the mass flow rate is displayed in Fig. 10 and its behavior can be described by a quadratic function for the whole domain.

Besides the performance of the pressure, both Figs. 9 and 10 show the pressure after the pump and the pressure before the nozzle. As it was expected, the pressure after the pump is higher than the pressure before the nozzle. Nevertheless, the pressure does not fall considerably, despite the length and continuous curvature of the hose. The percentage of the pressure loss due to the hose is shown in Fig. 11. This figure shows that the pressure loss is lower than 10% and that the percentage decreases when the diameter of the nozzle is reduced.

Taking into account that the characteristics of the nozzle do not change, it is possible to calculate the resistance coefficient generated with each nozzle with the application of Eq. 5, where ΔP is in Pa, ρ is 1000 kg/m^3 and v is in m/s. The calculated values are displayed in Fig. 12, and this figure shows that the growth of this coefficient can be described with the power function $K = 880.14d^{-3.842}$. This function considers the effects of the abrupt change of direction and the reduction in the diameter of the orifice, even though the diameter is the only variable that changes. Considering the behavior of the function, it can be deduced that the diameter of the orifice is the element

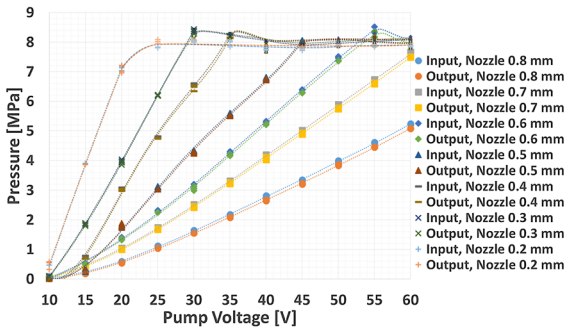

Fig. 9 Description of the pressure at the ends of the hose generated with different diameters of the outlet at different voltages supplied to the pump. The pressures at the input and output of the hose differ slightly and reach a maximum value of around 8 MPa

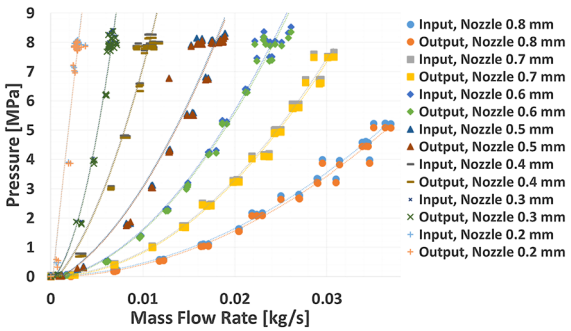

Fig. 10 Description of the pressure at the ends of the hose generated with different diameters of the outlet at different mass flow rates. The description of the pressure with a variable that does not depends on the pump allows to have a better description of the behavior

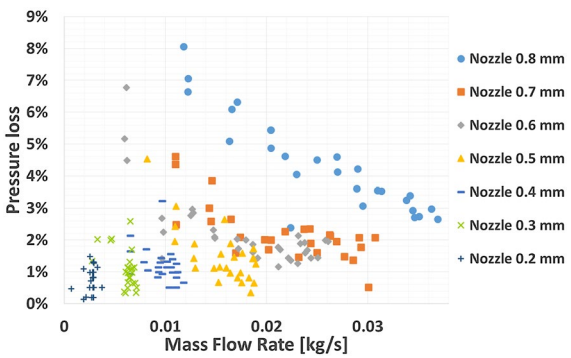

Fig. 11 Description of the percentage of pressure loss generated with different diameters of the outlet at different mass flow rates

that more contributes to the resistance coefficient value since the change of direction keeps constant.

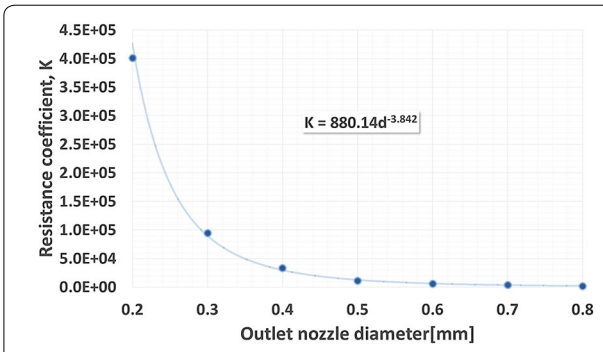

Fig. 12 Resistant coefficient of the nozzle at different diameters of the outlet

Thrust force measurement

The better way to describe the behavior of the variables of interest is with respect to a variable independent from the pump performance. However, since we control the system through the voltage supplied to the pump, it is necessary to describe the thrust force with respect to this variable. This description is shown in Fig. 13 and it shows that the maximum force reached is around 3.5 N. This force is reached only with the nozzles of diameters of 0.7 and 0.8 mm. In a similar way as it happened with the mass flow rate, for the nozzles from 0.2 to 0.6 mm, the thrust force increases with the voltage. However, at some point, the force tends to keep constant. The behavior of the thrust force with respect to the input voltage of the pump before it reaches the steady value can be described through polynomial functions of degree three. However, as it was mentioned before, this behavior will be only observed with pumps having the same characteristics as the one employed in the experiment.

In order to generalize the results of the thrust force regardless the pump used, this force is described in function of the mass flow rate as is shown in the Fig. 14. In this general description, second order functions have the best matching to describe the behavior. With this chart, it is easier to visualize that the increasing rate of the thrust force is larger the smaller the diameter of the nozzle. However, the smaller the diameter of the orifice, the smaller the maximum thrust force that can be reached. This is due to the mechanical limitation that the pump has, which is reached easily with the smallest nozzles because the pressure increases rapidly.

With the thrust force acquired experimentally and the data of the mass flow rate, it is possible to calculate the percentage rate of the thrust force generated due to the momentum of the water flowing through the input and output of the nozzle by using Eq. 3. The results of this calculation are visualized in Fig. 15 and show that the larger the diameter of the orifice in the nozzle, the larger

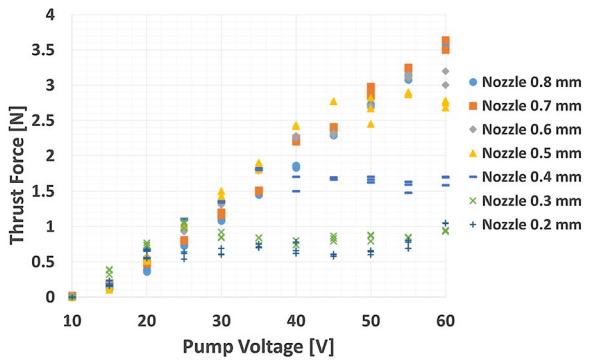

Fig. 13 Description of the thrust force generated with different diameters of the outlet at different voltages supplied to the pump

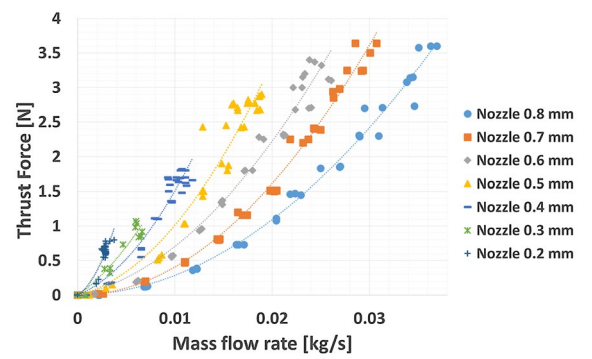

Fig. 14 Description of the thrust force generated with different diameters of the outlet at different mass flow rates

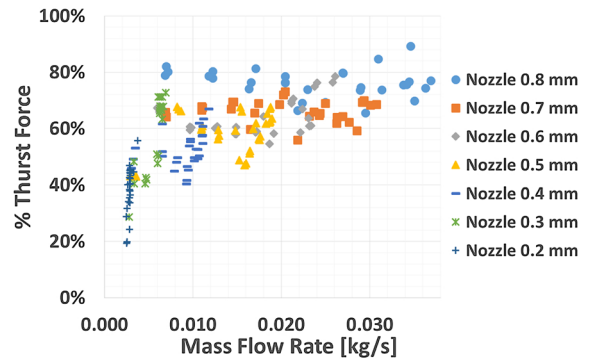

Fig. 15 Percentage of pressure loss due to the hose generated with different diameters of the outlet at different mass flow rates

the contribution of the flow of water inside the nozzle for the generation of thrust force. This contribution is more steady for larger diameters of the orifice, where the percentage of the thrust force can reach values up to 90% of the total force. Meanwhile for smaller diameters the percentage varies more and it can fall to values as low as 20%.

From the percentages shown in Fig. 15, just a small part corresponds to the force generated by the flow of water at the input of the nozzle. The maximum percentage of force that the flow at the input contributes is up to 2% and it only occurs with the orifice of 0.8 mm. Finally, considering all the variables that generate thrust force; flow at the input, flow at the output and pressure; the flow at the output is the one that tends to be the main source of propulsion. However, this contribution decreases with the reduction of the nozzle orifice.

Summary of water-jet experiments

After the experimentation with the test apparatus, we found out that despite that the reduction in the diameter of the orifice increases the speed of the fluid, the flow rate decreases at a larger rate and, consequently, the thrust force did not increase as expected. Furthermore, the main limitation for the thrust force is the maximum pressure that the pump is able to bear. The pressures developed are relatively large, however, they generate a reduced part of the thrust force. Meanwhile, the flow of water at the outlet is the main source for the thrust generation. It could be considered that a large flow with small pressure is preferable. In the analysis of the system, we found this characteristics with the nozzle of 0.8 mm and this diameter was chosen for the prototype. Furthermore, with the nozzles of diameter smaller than 0.5 mm, it was necessary to use filtered water since the tap water contains small particles that block the nozzle. Practically speaking, larger diameter is preferable to avoid this problem.

A larger diameter could further reduce the pressure, however, this may not bring enough advantages since the thrust force is not going to increase any further due to the limitation of the pump, as shown by its behavior in Fig. 13. Moreover, considering the behavior of the mass flow rate shown in Fig. 8, an incremental in the consumption of water is expected. Another possible way to optimize the thrust force is by increasing the flow without increasing the pressure is avoiding abrupt changes of direction in the nozzle and with a gradual reduction of the output instead of the orifice. Even so, these changes require a complex manufacturing in a reduced space, that could make it not feasible.

Finally, we found that despite the reduction in the diameter of the orifice, the speed of the water and consequently the water-jet thrust force did not increase as expected because the resistance factor incremental reduces the mass flow rate. Furthermore, this resistance incremental makes that the pressure elevates faster and the mechanical limitations of the pumps are reached faster as well.

Hardware design

As was mentioned before, the configuration of three nozzles with three independent pumps was chosen because this design allows a straightforward implementation to test the water-jet propulsion. In this configuration, we used three identical hoses that have identical nozzles attached. Hoses used in this prototype have the same characteristics as the composite hose used in the test apparatus. However, the length for the prototype increased to 40 m. The nozzle has a single output hole with a diameter of 0.8 mm which is directed backward with an angle of 45° with respect the longitudinal axis of the hose, as is shown in Fig. 16a. The three hoses are attached rigidly through all their length. The hoses together have a diameter of about 20 mm. The output holes of nozzles are directed to outside with a separation of 120° between each other. This arrangement is displayed in Fig. 16b, c. The diameter of 0.8 mm for the nozzle was selected since this diameter generated the maximum thrust force with the minimum increase of pressure in the system. The pumps used to propel the water are the same as the one used in the test apparatus.

With the three water-jets controlled independently, it is possible to generate spatial motion. However, as happens in all the underactuated systems, a sequence of movements are necessary to reach some points, since it is not possible to reach them with direct motions. In particular for our configuration, due to the disposition of the water-jets nozzles, there is not any control on the rotation on the longitudinal axis of the probe. This necessitates either the addition of a mechanism that allows fixing of the orientation of the nozzles relative to a fixed reference or a sensor that acquires the attitude of the nozzles in order to do the corresponding compensation depending on the current orientation.

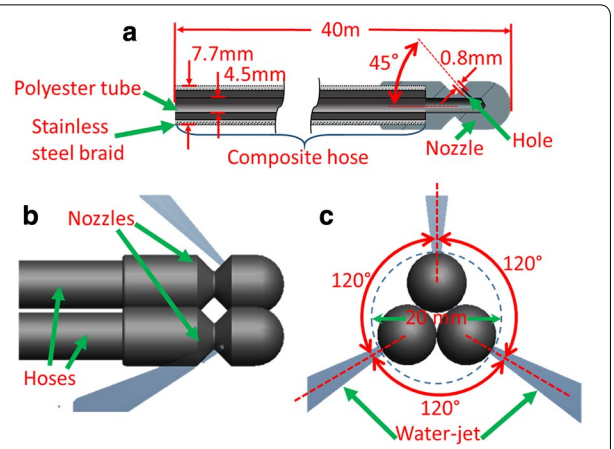

Fig. 16 Schematic of a single hose and disposition of the hoses at the tip of the device. **a** Lateral cut view of hose and its connection with the nozzle. **b** Lateral view of the three nozzles and water-jets disposition. **c** Frontal view of three nozzles and water-jets disposition

Electronic design

Four main elements for the electronic design were considered: user interface, sensing, processing, and power stage. Taking into account that a straightforward control is desired, a three axes joystick (Sakae 30JH) is used as the interface for the user. The three signals acquired from the joystick allows defining the direction of the movement, as well as the magnitude of the thrust force.

Considering the lack of control in the longitudinal axis and that any kind of mechanism to fix the orientation of the nozzle to an inertial frame will increase the dimensions of the device, we decided to use an inertial-measurement unit (IMU) at the tip in order to acquire the attitude at any moment. In particular, the IMU used has a 3D accelerometer, 3D magnetometer as well as three-axis gyroscope. Even though the calculation of the attitude is possible by using the data from only the gyroscope, we decide to integrate the data of all the sensors embodied in the IMU to have more precise values. Furthermore, depending on the requirements of the task, other sensors can be added. For instance: thermometer, camera, dosimeter, and so on.

Because the location of the IMU is far from the base of the system, it is better to perform the processing of its information nearby the tip. Furthermore, taking into account that the data needs to be sent to the base as well as protected as much as possible from electromagnetic noise, one of the best options to transmit the data is through CAN bus. Therefore, a microcontroller is necessary at the tip to process the information from the IMU and for the adaptation of the resultant data to be sent by CAN protocol. For that reason, we selected the HiBot TiTech M4 Controller board, which possess all the required elements mentioned before. At the base of the probe, another microcontroller is required to receive the information from the TiTech M4 and process the attitude data together with the information of the desired direction of motion sent by the user through the joystick. For this task, we chose the HiBot TiTech SH2 Controller board.

By using CAN standard, we can reduce the weight of the whole cable because this communication can be done with a few wires. In particular, for our system, we decide to use shielded cable with two pairs of inner twisted cables. One pair transmits the High and Low CAN signals and one cable from the second pair is used as the ground reference. The other cable in the second pair is used together with the shield to transmit power to the microcontroller. This configuration allows the connection of several nodes. Additionally, due to the differential

signaling used in this protocol, the data is protected against environmental noise. It is important to adjust the bitrate communication depending on the length of the cable, having a max rate of 1000 kbit/s. In particular, we adjust the bit rate communication to 500 kbit/s since the total length of our cable is 50 m. Considering that the TiTech M4 is located at the tip, this and its connection with the cable must be waterproof. Thus, in order to avoid increasing the weight and size at the tip, a silicone case that completely covers the microcontroller was manufactured. Figure 17 shows the TiTechM4 inside the silicone case while testing the water seal and the final disposition at the tip of the system.

Finally, the power stage consists of three independent motor drivers (HiBot 1XH Power Module) and a universal motor for each pump. Each driver is fed with independent signals from the TiTech SH2, which processes the signals from the joystick and the IMU. After the signals are received, they are processed and converted to a Pulse Width Modulation signal (PWM), whose duty cycle regulation allows the control of the angular speed of the universal motor. The organization of all electronic elements are condensed in Fig. 18.

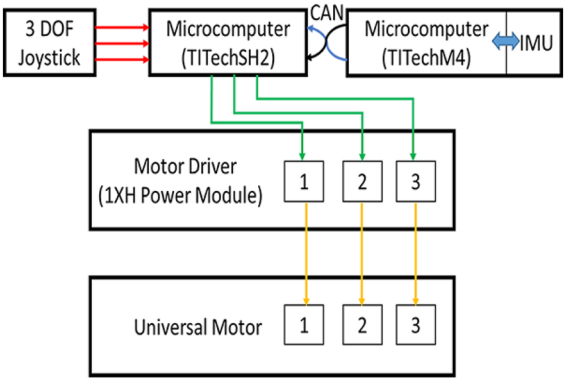

Fig. 18 Schematic of the electronic system

Control design

The movement of the tip is controlled through the regulation of the flow rate which directly modifies the thrust force of each water jet. Therefore, as is shown in the local reference system of Fig. 19, the direction of the movement can be established by the vectorial summation of the thrust forces of the three water-jets. After normalizing the magnitude of the thrust force of each water jet, the calculation of all the possible magnitudes and directions of the total thrust force is done. The family of the final points of all the thrust force vectors calculated is displayed in Fig. 20. This figure shows that the whole family of points is contained inside a cube. The points of maximum and minimum thrusting force are located on the red and blue vertices of the cube, which coincide with the longitudinal axis of the probe as well.

Since the orientation of this cube is fixed to the orientation of the nozzles and the field of force vectors is not symmetrical on the longitudinal axis, the correction of the propulsion, when a rotation on this axis is presented could generate some difficulties. Due to the lack of symmetry in vectors field, at some changes of orientations, it

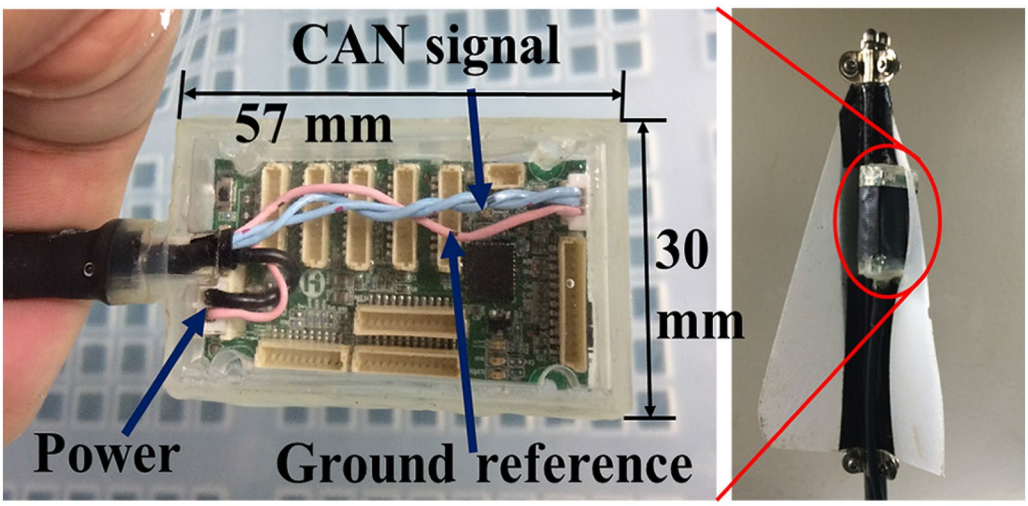

Fig. 17 TiTech M4 with cable connectors inside the silicone case. **a** Dimension of the silicon case and connection with the communication cable. **b** Final position of TiTech M4, the fins are installed to increase the protection to the microcontroller

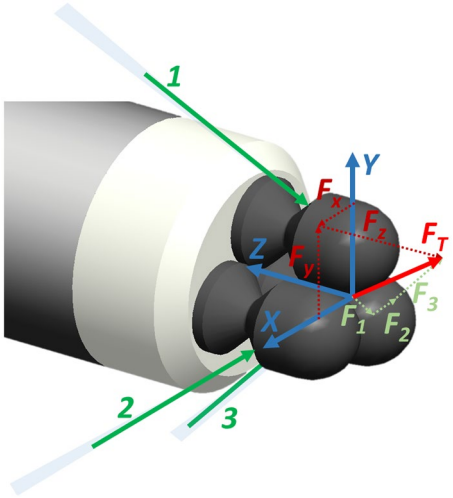

Fig. 19 Orientation of the local reference system placed at the tip and vectorial summation for the total thrust force. The *light green vectors* represent the thrust force of each water-jet and the *dark red vector* represent the projection of the total thrust force on the local reference system

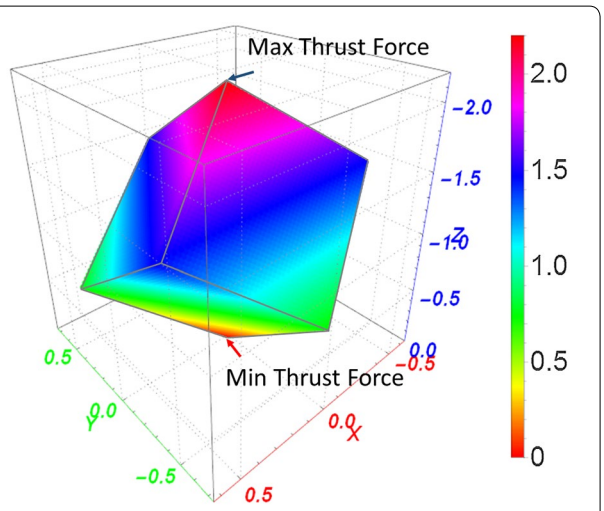

Fig. 20 Family of total thrust force generated by the normalized force of each water-jet. The origin of all the family of vectors is located at 0, 0, 0 and the final point of all the vectors is located inside the cube

is not possible to generate all the vectors with respect to the inertial orientation, especially those located nearby the edges of the cube. Taking into account that the control is done through a joystick, one way to solve the problem of lack of symmetry and to better relate the thrust force vector field with the motion of the joystick is by reducing the force field shown in Fig. 20. We propose the limitation of the low magnitude vectors of the field with a cone as is displayed in Fig. 21. The aperture of the cone is defined by the maximum angle that allows the cone to be completely contained inside the lower half of the cube. In this case, the aperture angle is 53.13°. This angle allows us to decrease as little as possible the vector field of the low half. While it is possible to delimit the whole vector field with two cones connected by their base, we only delimited the lower magnitude zone to avoid reducing, even more, the vector field. This allows for more accurate control of the device with the forces contained in the low magnitude zone, which fits better with the motion of the joystick. Meanwhile, in the zone of higher magnitude forces, the complete range of thrust forces that the system can generate are available. Nevertheless, for these zone, the precision of the control is reduced due to the reduction of similarity with the field of motion of the joystick.

In regard to the control of the whole device, we decide to adopt a control similar to the radio-control cars, since, like them, our system is underactuated and a forward motion is generated in order to move sideways. The main difference is that our device can move in three-dimensional space. The x-axis from the joystick represents the horizontal motion, meaning left-right motion, and the y-axis represent the vertical motion, meaning the up-down motion. This two motions are defined on a local reference frame that is located at the tip of the probe, which moves all the time with the probe and keeps its y-axis perpendicular to the ground of the user: the inertial reference frame. Finally, the z-axis of the joystick controls the magnitude of the thrust force. As a result, through the attitude obtained via the IMU, the flow of the pumps is adapted automatically to any orientation that the probe has, in order to fulfill the motion in the wanted direction. We also chose this strategy of control because up to this point in the design, there is no camera installed on the probe and the operator needs to keep sight of the position of the probe. Later, when a camera is installed at the tip of the probe, this control can be modified in order to define all the motions completely with respect to the local reference system located at the tip of the probe.

In order to probe the efficiency of the designed control and the correction of the rotation in the longitudinal axis, the motion of a small section of the probe was tested inside a water tank. As is shown in Fig. 22a, the hose was attached rigidly about 0.3 m behind its tip. Afterward, a circumference was traced with the joystick. This circumference had the maximum diameter available in the joystick and the z-axis kept the maximum value all the time. We verified that the tip of the system consistently followed the motion of the joystick and generated a circumference with an approximate diameter of 0.3 m, as is displayed in the sequence photography in Fig. 22b. The same figure shows the rotation of the tip and the joystick

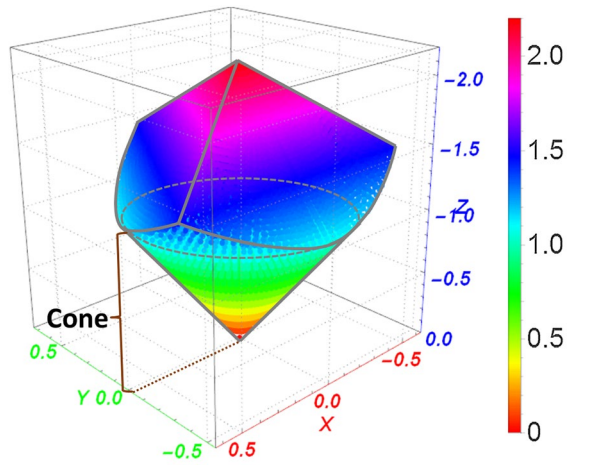

Fig. 21 Field of vectors delimited with a cone in the low range magnitude

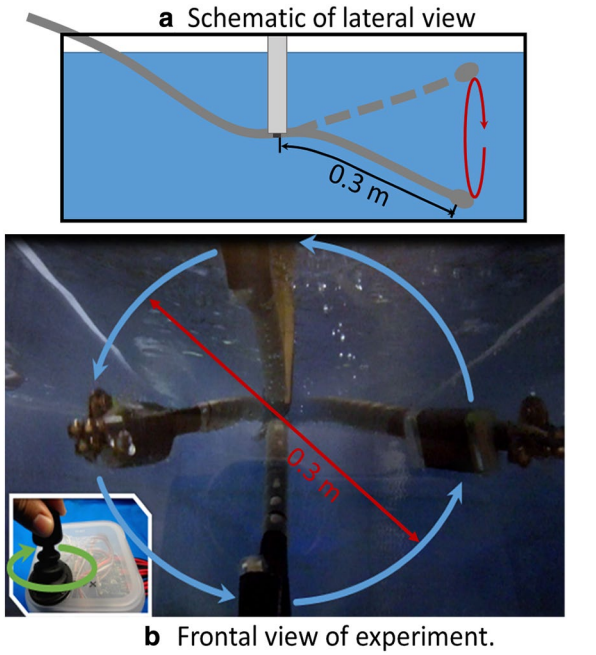

Fig. 22 Test of the control of the device to verify that the movement of the system follows the motion of the joystick. **a** The probe was attached rigidly 0.3 m behind its tip to test the effectiveness of the control. **b** With the fixation restriction, we were able to generate circumferences of 0.3 m applying maximum thrusting force with the maximum inclination in the joystick for different longitudinal orientation of the probe

in opposite directions because the view of the sequence shot of the tip was taken from the front. In this experiment, where the system is attached rigidly, the diameter of the circumference traced by the probe can be defined through the inclination of the joystick or through the magnitude of the water jet. The experiment was repeated several times changing the longitudinal orientation of the system. Regardless the change in the orientation, the system did not lose the reference due to the continuous correction in the orientation done with data gathered from the IMU. Repetitiveness of the control was also verified since circumference with similar diameters were generated for all the orientations tested.

Maneuvering experiments

Tests were conducted in different environments to simulate more typical conditions such as: on the ground (pavement), in air, and in water.

Regarding the test on the ground, two targets cones were placed seven meters from each other. The aim of the test was to touch the two targets with the tip of the probe. As is displayed in Fig. 23a, the starting position of the tip of the probe was in the middle of the two targets and three meters in a perpendicular direction from an imaginary line that connects the cones. A restriction of continuous contact between the probe and the ground was also established in order to verify the performance of the system in two-dimensional motion. Through the experiment, the longitudinal orientation of the system changes occasionally when the probe starts to move on the ground due to the friction or due to the intrinsic rigidity of the hoses. Despite the fact that it was possible to reach both targets in less than 1 min, different issues related to the friction were presented. Due to the large contact that the probe had with the ground, the thrust force generated by the water-jet was not strong enough to propel forwards in a straight line. Therefore, we employed a strategy based on moving the tip laterally from side-to-side in order to gather the momentum necessary for the forward motion. This lateral motion done by the system resembles a snake-like motion. Even though this motion helped to overcome the friction force, there is a limit on the total length that the probe can be moved with this strategy, which is less than 7 m. Because the lateral motion to gather momentum varies depending on the friction factor between the surfaces in contact, it is not possible to measure an average speed of this motion. Figure 23b displays a sequence of images of the experiment.

With respect to the motion in the air, an identical task as for the test on the ground was established, the main difference resided in keeping the tip of the probe in the air at all times. During experimentation, it was possible to raise about 1 m of the probe to an approximate height of 0.4 m, as is shown in the sequence shot in Fig. 24. The tip of the probe glided in the air with no time limit. However, because the contact between this part of the probe and the ground did not exist, the motion of the tip became

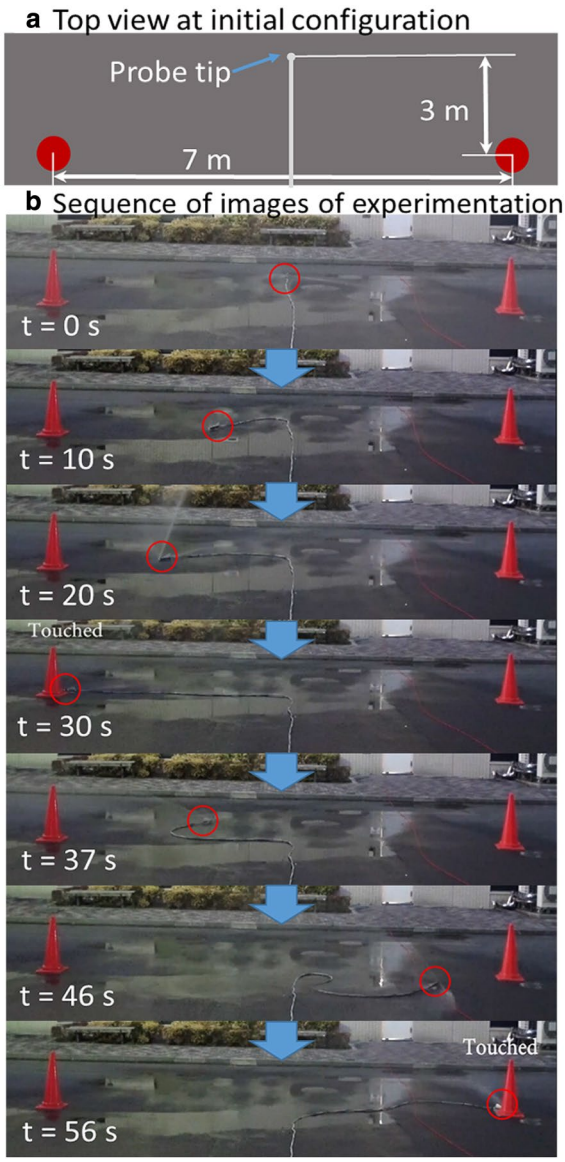

Fig. 23 Test of the motion of the device on the ground. **a** Initial position of the probe with respect to the target cones. **b** Location of the tip at different moments during experimentation

sensitive and difficult to control; with just a small change in direction in the joystick, the tip moved abruptly to that direction. In fact, due to this reason, it was difficult to fulfill the task. In general, the rest of the probe stayed motionless on the ground. However, as happened in the experimentation on the ground, while the tip is moving in the air it was possible to gather momentum and drag part of the probe. Despite the issues encountered in the experimentation, it was possible to verify the immediate recovery of reference anytime the probe rotates abruptly on its longitudinal axis.

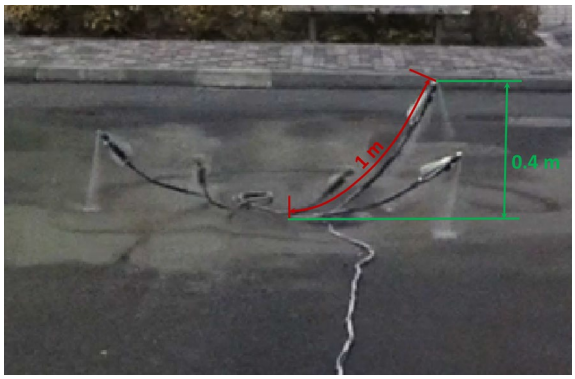

Fig. 24 A sequence shot of the experimentation of motion of the device in the air. About 1 m of the device was possible to raise in the air to a maximum height of 0.4 m

For the experiments inside the water, initially, we tested the motion of the probe without the TiTech M4 and the communication cable. In these experiments, due to the homogeneity of the environment, the probe moved easily inside the water and the resistance force of the water was small enough to allow forward displacements without the need of snake-like movements. Furthermore, it was possible to pull around 20 m of the probe in straight line motion. We noticed that the friction was large enough to avoid the impulsive motion in three-dimensional displacement. However, the problem of lack of control in the longitudinal axis was more evident because the probe tended to rotate a lot on this longitudinal axis and, consequently, the reference was easily lost. Therefore, the TiTech M4 was installed to solve this problem. However, with the TiTech M4 and the communication cable installed, the weight of the device was increased and the buoyancy force reduced. Hence, some pieces of Styrofoam were added along the probe in order to increase the buoyancy. After this addition, the reduction of buoyancy force was solved and the probe was able to move without any problem as before. Finally, in order to comprehensively test the motion and controllability of the probe submerged in water, three different targets were placed at the bottom of a pool with a depth of 2 m. These targets had a separation distance of around 3 m from each other and a fourth target was placed on the surface. The approximate position and the time taken to reach each target are shown in Fig. 25. Due to the homogeneity of the environment and the presence of a larger drag force, the motion and control of the system were easier and accurate. There was not need for a special strategy for the motion and all the target were reached without any problems. For the purpose of moving the probe in a straightforward way and reduce the number of turns to reach every target, when necessary, the user pulled back

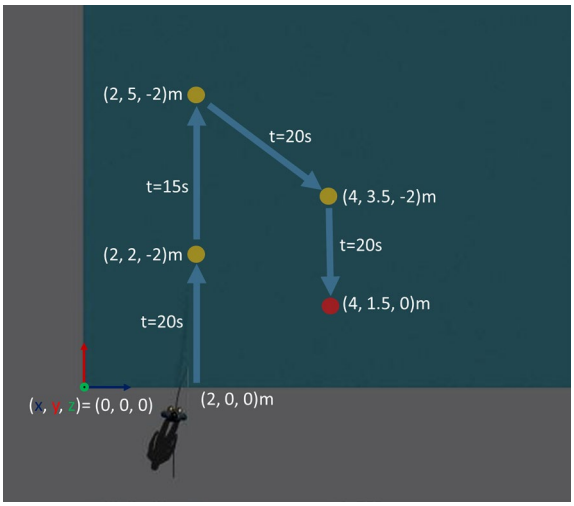

Fig. 25 Schematic top view of the positions of the targets in the pool. Position described in meter from the corner of the pool and the time required to reach every target

the probe from outside the pool with the purpose of adding a backward motion. Moreover, a maximum speed of 0.5 m/s on a straight line was measured. Figure 26 displays some images of the experiments performed in the water.

The usefulness and efficiency of the IMU to correct the lack of control in the longitudinal axis was more notorious in the experiments carried out in the air and inside the water. The reason is that, in these environments, the device has less restriction to rotate and lose its reference. The IMU also helped to more easily control the system because the orientation of the reference frame at the tip was partially adapted to the reference of the user.

Discussion

In general, the use of the IMU to acquire the orientation at the tip as well as the delimitation in the thrust force field allows us to control the system in different environments in a straightforward way. Nevertheless, the motion on the ground requires the implementation of snake-like motion, which is necessary to overcome the limitation generated by the large friction force. Another way to overcome this limitation is by using more powerful pumps since the pumps used in the experiments belong to middle-range-pressure washing machines aimed at home use. On the other hand, in the tests done with the probe in the air, we were able to keep the tip gliding in the air. However, the control was extremely sensitive and just a small change of direction in the joystick caused an impulsive motion at the tip. This made it very difficult to direct the probe to a fixed point due to the lack of drag force. A possible way to solve this problem is by the implementation of a PID control in order to damp the impulsive motion that is generated when the probe is in the air. The experiment in the pool helps us to understand that in order to make it easier to control our system, an extra degree of freedom that pulls the probe backward may be useful. This degree of freedom could be added by the addition of a motorized reel which collects the probe when it is necessary. Finally, although the developed probe is larger than the grating hole due to the size of the IMU, we can minimize its size by custom

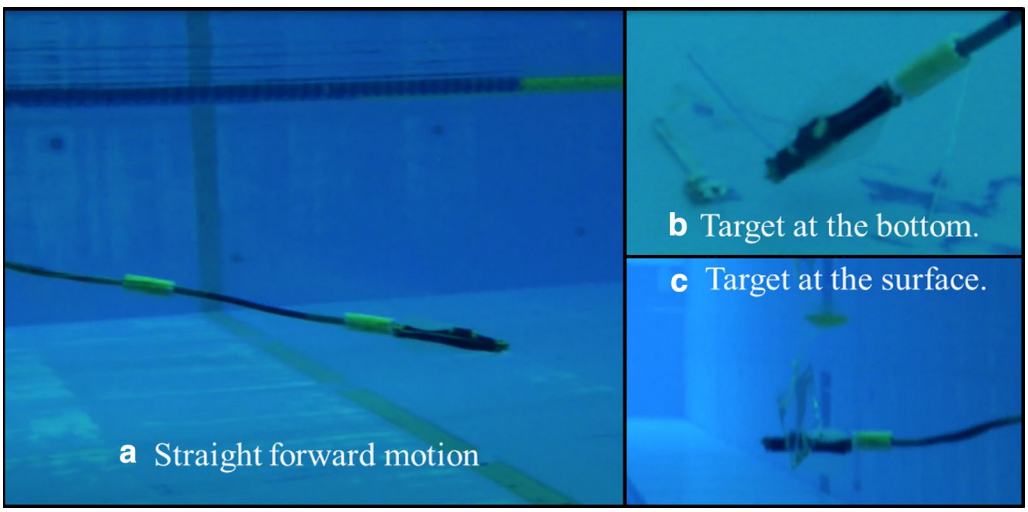

Fig. 26 Test of the motion of the device inside the water at different depths. **a** It was possible to reach a speed of 0.5 m/s and pull up to 20 m of the device in straight line. **b** The searching of several objects at 2 m of depth was carried out. **c** The change of depth from the bottom to the surface is performed without problem

made in the near future. In the current device, we use a commercially available IMU for ease implementation.

Conclusion

In this paper, we propose the usage of water-jet as propulsion source with the aim of solving the need of developing more slender and longer devices for inspection tasks. An analysis of the variables that interact in the generation of thrust force was developed with the intention of understanding their correlation. We found that the main limitation for the thrust force is the maximum pressure that the pump is able to bear. A first prototype was developed to test the mobility and controllability of the device on the ground, in the air and under water. It was possible to move and control the device on the ground, in the air and under the water. However, in the aquatic environment, the system shown the best controllability and mobility. Finally, the water jet seems promising to be used as propulsion source for inspection systems, however, further research is necessary to improve and explore different possibilities of this concept.

Authors' contributions

All authors equally contributed. All authors read and approved the final manuscript.

Author details

[1] Department of Mechanical and Aerospace Engineering, Tokyo Institute of Technology, 2-12-1 Ookayama, Meguro-ku, Tokyo 152-8550, Japan. [2] Hibot Corp., 5-9-15 Kitashinagawa, Shinagawa-ku, Tokyo 141-0001, Japan.

Competing interests

The authors declare that they have no competing interests.

Received: 5 November 2016 Accepted: 22 February 2017
Published online: 07 March 2017

References

1. Moore T (1985) Robots for nuclear power plants. Int Atomic Energy Agency Bull 27(3):31–38
2. Seward DW, Bakari MJ (2005) The use of robotics and automation in nuclear decommissioning. In: 22nd international symposium on automation and robotics in construction, vol. 44. ISARC, Ferrara, Italy
3. Roman HT (1991) Robots cut risks and costs in nuclear power plants. IEEE Comput Appl Power 4(3):11–15. doi:10.1109/67.85957
4. Fischetti MA (1985) Robots do the dirty work: Some walk, some roll as they go about their tedious, hazardous chores in nuclear-power plants. IEEE Spectr 22(4):65–73. doi:10.1109/MSPEC.1985.6370621
5. Sugisaka M (2011) Working robots for nuclear power plant desasters. In: 5th IEEE international conference on digital ecosystems and technologies (IEEE DEST 2011), vol 5, pp 358–361. IEEE, Daejeon, South Korea. doi:10.1109/DEST.2011.5936593
6. TEPCO: TEPCO application of robot technology. http://www.tepco.co.jp/en/decommision/principles/robot/index-e.html. Accessed 10 Sept 2016
7. Tokyo Electric Power Company: Investigation results of inside the Fukushima Daiichi Power Nuclear Plant Unit 2 Primary Containment Vessel (PCV)-Guide Pipe removal-. Technical report, TEPCO (2013). http://www.tepco.co.jp/nu/fukushima-np/handouts/2013/images/handouts_130422_06-j.pdf (in Japanese)
8. Robinson G, Davies JBC (1999) Continuum robots—a state of the art. In: Proceedings 1999 IEEE international conference on robotics and automation (Cat. No.99CH36288C), vol 4, pp 2849–2854. IEEE, Detroit, Michigan, USA (1999). doi:10.1109/ROBOT.1999.774029
9. Rolf M, Neumann K, Queißer JF, Reinhart RF, Nordmann A, Steil JJ (2015) A multi-level control architecture for the bionic handling assistant. Adv Robot 29(13):847–859. doi:10.1080/01691864.2015.1037793
10. McMahan W, Chitrakaran V, Csencsits M, Dawson D, Walker ID, Jones BA, Pritts M, Dienno D, Grissom M, Rahn CD (2006) Field trials and testing of the OctArm continuum manipulator. In: Proceedings 2006 IEEE international conference on robotics and automation, 2006. ICRA 2006, pp 2336–2341. IEEE, Orlando, Florida. doi:10.1109/ROBOT.2006.1642051
11. Buckingham RO, Graham AC (2010) Dexterous manipulators for nuclear inspection and maintenance—case study. In: 2010 1st international conference on applied robotics for the power industry (CARPI 2010), pp 1–6. IEEE, Montréal, Canada. doi:10.1109/CARPI.2010.5624476
12. Mehling JS, Diftler MA, Chu M, Valvo M (2006) A minimally invasive tendril robot for in-space inspection. In: The first IEEE/RAS-EMBS international conference on biomedical robotics and biomechatronics, 2006. BioRob 2006, vol 2006, pp 690–695. IEEE, Pisa. doi: 10.1109/BIOROB.2006.1639170
13. Walker ID (2013) Robot strings: long, thin continuum robots. In: 2013 IEEE aerospace conference. IEEE, Big Sky, Montana, pp 1–12. doi:10.1109/AERO.2013.6496902
14. Buckingham R, Graham A (2012) Nuclear snake arm robots. Ind Robot Int J 39(1):6–11. doi:10.1108/01439911211192448
15. Horigome A, Yamada H, Endo G, Sen S, Hirose S, Fukushima EF (2014) Development of a coupled tendon-driven 3D multi-joint manipulator. In: 2014 IEEE international conference on robotics and automation (ICRA). IEEE, Hong Kong, China, pp 5915–5920. doi: 10.1109/ICRA.2014.6907730
16. Fukuda J, Konyo M, Takeuchi E, Tadokoro S (2014) Remote vertical exploration by active scope camera into collapsed buildings. In: 2014 IEEE/RSJ international conference on intelligent robots and systems. IEEE, Chicago, Illinois, USA, pp 1882–1888. doi:10.1109/IROS.2014.6942810
17. Shinsho: Shinsho Nozzles. http://www.ss-shinsho.co.jp/nozzle.html. Accessed 16 Sept 2016
18. Fricke: Lindauer Schere. http://www.fricke-kanal.de/Leistungen/TV-Inspektion/Lindauer-Schere/lindauer-schere.html. Accessed 16 Sept 2016
19. Jetlev-Flyer. http://jetlev-flyer.com/. Accessed 16 Sept 2016
20. Zapata Racing. http://zapata-racing.com/en/. Accessed 16 Sept 2016
21. Wu G, Sun H, Zou J, Wan L (2009) The basic motion control strategy for the water-jet-propelled USV. In: 2009 international conference on mechatronics and automation. IEEE, Changchun, China, pp 611–616. doi:10.1109/ICMA.2009.5245049
22. Guo S, Lin X, Hata S (2009) A conceptual design of vectored water-jet propulsion system. In: 2009 International conference on mechatronics and automation. IEEE, Changchun, China, pp 1190–1195. doi:10.1109/ICMA.2009.5246462
23. Mazumdar A, Lozano M, Fittery A, Asada HH (2012) A compact, maneuverable, underwater robot for direct inspection of nuclear power piping systems. In: 2012 IEEE international conference on robotics and automation. IEEE, Saint Paul, Minnesota, USA, pp 2818–2823. doi:10.1109/ICRA.2012.6224619
24. Tokyo Electric Power Company: Investigation result of inside of the Primary Containment Vessel (PCV), 1F-2. Technical report, TEPCO (2012). http://www.tepco.co.jp/en/nu/fukushima-np/roadmap/images/m120123_01-e.pdf
25. Tokyo Electric Power Company: Summary of Decommissioning and Contaminated Water Management. Technical report, TEPCO (2015). http://www.tepco.co.jp/en/nu/fukushima-np/roadmap/images/d151001_01-e.pdf
26. Tokyo Electric Power Company: Development of a technology to investigate inside the Reactor Primary Containment Vessel (PCV)-Site test "Investigation B1" on grating around the pedestal inside Unit 1 PCV-. Technical report, TEPCO (2015). http://www.tepco.co.jp/en/nu/fukushima-np/handouts/2015/images/handouts_150406_01-e.pdf